

---

# HandS3C: 3D Hand Mesh Reconstruction with State Space Spatial Channel Attention from RGB images

---

**Zixun Jiao**

Xi'an Polytechnic University

**Xihan Wang**

Xi'an Polytechnic University

**Zhaoqiang Xia**

Northwestern Polytechnical University

**Lianhe Shao**

Xi'an Polytechnic University

**Quanli Gao**

Xi'an Polytechnic University

## Abstract

Reconstructing the hand mesh from one single RGB image is a challenging task because hands are often occluded by other objects. Most previous works attempt to explore more additional information and adopt attention mechanisms for improving 3D reconstruction performance, while it would increase computational complexity simultaneously. To achieve a performance-reserving architecture with high computational efficiency, in this work, we propose a simple but effective 3D hand mesh reconstruction network (i.e., HandS3C), which is the first time to incorporate state space model into the task of hand mesh reconstruction. In the network, we design a novel state-space spatial-channel attention module that extends the effective receptive field, extracts hand features in the spatial dimension, and enhances regional features of hands in the channel dimension. This helps to reconstruct a complete and detailed hand mesh. Extensive experiments conducted on well-known datasets facing heavy occlusions (such as FREIHAND, DEXYCB, and HO3D) demonstrate that our proposed HandS3C achieves state-of-the-art performance while maintaining a minimal parameters.

## 1 Introduction

The reconstruction of 3D hand mesh from one single RGB image has a wide range of applications in many fields, such as VR/AR, robotics, and human-computer interaction. 3D hand mesh reconstruction based on RGB images for the reconstruction has attracted much attention due to its low cost and computational friendliness. Influenced by the rapid development of deep learning, many excellent works [17, 1, 7, 16, 48, 37, 27] have emerged in this field. These works focus on important issues related to hand-object occlusion and the loss of local information. Despite significant advancements, most methods still struggle to reconstruct hand poses in scenarios with substantial occlusion or when the prior knowledge is not sufficient.

The previous methods can be broadly categorized into two categories. One is to incorporate additional prior knowledge. To cite few, Zimm et al. [53] obtained hand region features via a hand segmentation network. Wang et al. [48] added keypoint coordinates as strong prior information to constrain hand pose. These methods can enhance pose reconstruction performance, but lack essential prior information in practical applications. Another category is to learn the intrinsic connection between

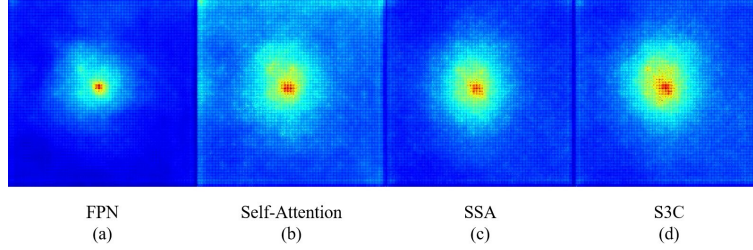


Figure 1: Effective receptive fields (from left to right: FPN, Self-Attention, State Space Attention (SSA) and State-Space Spatial-Channel Attention (S3C)).

image features through deep networks, Park et al. [37] extracted the complete hand information by distinguishing the features. Jiao et al. [23] used the Transformer architecture to obtain the global information and expect to learn the hand feature mapping from the occluded part. These methods tend to mine the association between image features, but there are still some limitations. First, the attention mechanism leads to excessive computational complexity. Second, an overload of global information can interfere with the effective receptive field [32], as shown in Figure. 1 (b).

Based on the above observations, we propose a simple but effective 3D hand mesh reconstruction network called as **HandS3C**. This framework incorporates the state space model [31, 34, 43] into the field of hand mesh reconstruction for the first time. At the same time, combining the idea of spatial-channel feature fusion [20], **State Space Spatial Channel (S3C)** attention module is constructed to emphasize the contribution of channel-dimensional features. This not only increases the range of effective receptive fields in the network, but also effectively avoids the square-step computational complexity of traditional attention. Specifically, our main contributions are summarized as follows:

- (1) We design a 3D hand mesh reconstruction network called as HandS3C, which introduces the state space model to the task of hand mesh reconstruction for the first time. This network can effectively improve hand reconstruction performance without the need for additional prior knowledge.
- (2) We propose a spatial and channel-wise parallel scanning approach to compensate for the missing channel information in planar scanning. The state-space spatial-channel attention module is constructed, which can enhance the effective receptive field range while maintaining a small number of parameters.
- (3) Our method achieves state-of-the-art on three datasets, FREIHAND, DEXYCB and HO3D, with a small number of parameters.

## 2 Related work

### 2.1 Additional Information based Methods

It is difficult to restore 3D hand gestures from RGB image features alone, and most researchers use heatmaps [1, 33, 21], segmentation [53, 51], depth maps [40, 41, 49], and density maps [52, 4] to incorporate additional information to help the network better learn hand features in occlusion situations. In recent years, some scholars [48, 22] incorporate human prior knowledge to guide the network to focus on the target region, Wang et al. [48] proposed HandGCAT, which learns the prior knowledge of the hand joint positions through the knowledge-guided graph convolution module, and then through the cross-attention Transformer to guide the network to inject joint information into the occluded region. In addition, other scholars [17, 47, 39, 26, 3] have argued that the object pose affects the hand pose. To end this, Qi et al. [39] introduced Signed Distance Field (SDF) to reconstruct the occluded object and the hand, and this method is able to determine the grip state of the hand by estimating the object pose and then determining the hand’s grasping state.

### 2.2 Attention based Methods

Attention mechanisms have achieved great success in the field of deep learning, due to their ability to map long-term contextual relevance. In the task of hand mesh reconstruction, occluded hand features can be learned through global mapping with various attention modules, which in turn can effectively solve the occlusion problem [37, 27, 5, 11, 38]. In establishing the global context of hand-object

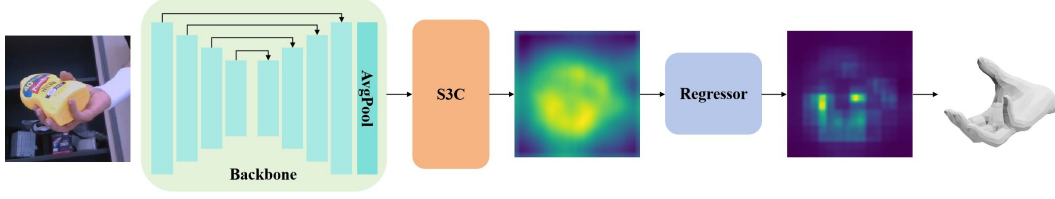


Figure 2: Overall architecture of HandS3C including Backbone, S3C and Regressor. HandS3C uses Resnet50 to extract image features and fuses multiscale features by upsampling layer by layer. It then uses S3C to obtain hand region features through parallel spatial and channel scanning. Finally, the regressor obtains keypoint information by heatmap encoding and outputs MANO parameters. The final 3D hand mesh is obtained by forwarding the MANO parameters to the MANO layer.

interaction, Pavlakos et al. [38] learn the mapping relationship between hand and occlusion from large-scale data through the Vision Transformer (ViT) architecture. Cho et al. [5] obtained the features related to the region of interest from the occluded portion through cross-attention. Park et al. [37] made full use of the information of occluded region as an enhancement of image feature of the hand and refine it to get the complete hand features.

### 2.3 State Space Model

With the proposal of attention mechanism [46], it makes more models can effectively focus on global information mapping, but its quadratic computational complexity leads to computational inefficiency in the case of long sequences. In the field of natural language processing, Gu et al. [13] proposed the S4 model to optimize the state space model (SSM) in order to solve the problems of computational efficiency and long sequence dependency. However, the S4 model would process all inputs in the exactly same way, which is not in line with the practical intuition that each sequence should receive different attention. Therefore, Gu et al. [12] introduced a selection mechanism to the Mamba architecture (S6) for learning the parameters in the traditional state-space model, through which it is able to focus on or ignore some sequences. Compared to traditional attention computation methods, S6 enables each element in a 1-D array (e.g., a text sequence) to interact with any previously scanned samples through a compressed hidden state, effectively reducing the quadratic complexity to a linear one. Influenced by this idea, Liu et al. [31] introduced it to vision tasks by combining the ViT model [9] to transform images into sequences, and proposed a cross-scanning module to solve the problem of image orientation sensitivity. This is made possible by the selectivity of the state space model, which allows it to enhance similar features in the hidden space. Therefore, we abstract the selective state-space model and the cross-scanning module therein into a state space attention (SSA) module, as shown in Figure. 1 (c). In addition, some researchers [43, 34, 8] have also combined state-space modeling with traditional CNN architectures to extract multi-scale global features in U-shaped structures by state-space selection modeling, and retained the deep-level information. In this paper, we introduce state space model into the field of hand mesh reconstruction for the first time, and design a state space spatial channel attention module (S3C). The module performs parallel scanning in both spatial and channel dimensions, and uses a selective state-space model to achieve feature selection in the hidden space. This method is able to extend the effective receptive field with a small number of parameters and focuses the network attention on the hand region, thus improving the accuracy of hand mesh reconstruction.

## 3 Methodology

### 3.1 Overview

The overall network architecture is shown in Fig. 2 and consists of Backbone, S3C and Regressor components. Given a hand image  $I \in \mathbb{R}^{256 \times 256 \times 3}$ . First, the appearance information is extracted by ResNet-50 based encoder-decoder and the multi-scale features are fused layer by layer to get the original feature map  $F \in \mathbb{R}^{256 \times 32 \times 32}$ . Then, it is fed into the S3C module and scanned in both spatial and channel dimensions to compute a 2D feature map and fused to obtain enhanced hand features  $H \in \mathbb{R}^{256 \times 32 \times 32}$ . Finally, the hand features  $H$  are passed to the Regressor to calculate the

keypoint heat map  $HM \in \mathbb{R}^{21 \times 32 \times 32}$  to predict the keypoint coordinates. For the final 3D hand mesh, we used the most popular MANO parametric hand [42]. It is an articulated hand network generated from differentiable functions that takes as input the parameters that control the shape  $\beta \in \mathbb{R}^{10}$  and pose  $\theta \in \mathbb{R}^{48}$  of the hand.

### 3.2 Backbone

In the original feature extraction part, we use ResNet-50 [19] to extract image information and fuse multi-scale features layer by layer [29] in an U-shape encoder-decoder structure. Specifically, when the input image size is  $256 \times 256 \times 3$ , the size of the first layer of features after ResNet-50 becomes  $128 \times 128 \times 128$ . In the subsequent layers, each layer of image features  $F_i \in \frac{H_i}{2^i} \times \frac{W_i}{2^i} \times C_i, i \in (1, 2, 3, 4), C_i \in (256, 512, 1024, 2048)$  is obtained by downsampling. Then, upsampling is performed and the image features  $F_i$  are incorporated layer by layer to get the last layer of feature extraction with size of  $256 \times 64 \times 64$ . Finally, the feature mapping map  $F \in \mathbb{R}^{256 \times 32 \times 32}$  is obtained by fusing the feature information through average pooling.

### 3.3 State Space Spatial Channel Attention Module

**State Space Models.** S4ND [36] was the first study to introduce state space models into the field of vision by enabling it to receive 2D image information through a simple extension of the S4 model. The S6 module proposed by Gu et al. [12] was shown in VMamba [31] to be able to capture the global feature information of 2D image features through a selective scanning mechanism enabling it to capture the global feature information of the 2D image features and maintain linear complexity. The state space model expects to map the input  $x(t) \in \mathbb{R}^L$  to the output  $y(t) \in \mathbb{R}^L$  through the implicit state  $h(t)$  and the parameter  $A \in \mathbb{R}^{N \times N}, B, C \in \mathbb{R}^N, D \in \mathbb{R}^d$  with the following equation:

$$h'(t) = Ah(t) + Bx(t), y(t) = Ch(t) + Dx(t) \quad (1)$$

In order to computationally achieve efficient operations [14], the ordinary differential equations above need to be transformed into discrete functions. Specifically, when the input size is  $X_i \in \mathbb{R}^{L \times d}$ , the discretization is performed following the following rule:

$$h_i = \bar{A}h_{i-1} + \bar{B}x_i, y_i = \bar{C}h_i + \bar{D}x_i, \bar{A} = e^{\Delta A}, \bar{B} = (e^{\Delta A} - I)A^{-1}B, \bar{C} = C \quad (2)$$

where  $B, C \in \mathbb{R}^{d \times N}$  and  $\Delta \in \mathbb{R}^d$ . In practice, we improve the  $\bar{B}$  approximation by means of a first-order Taylor series [12]:

$$B = (e^{\Delta A} - I)A^{-1}B \approx (\Delta A)(\Delta A)^{-1}\Delta B = \Delta B \quad (3)$$

Unlike traditional spatial state models, the S6 block introduces a selective scanning mechanism, where  $B, C \in \mathbb{R}^{bs \times L \times N}$ , and  $\Delta \in \mathbb{R}^{bs \times L \times d}$  can be obtained from inputs of size  $X \in \mathbb{R}^{bs \times L \times d}$ . This means that S6 can sense contextual information from the inputs and update the weights.

**Spatial-wise Selective Scanning.** Unlike textual information, image information contains 2D spatial information such as local texture and global structure, and it is difficult to obtain the contextual relationship of the local sense field of an image by scanning with a simple S6 module. The 1-D convolution is extended to 2-D convolution in S4ND [14], and this approach leads to the loss of the ability to dynamically update weights based on context. In VMamba [31], rows and columns are unfolded and scanned along in four different directions: top-left to bottom-right, bottom-right to top-left, top-right to bottom-left, and bottom-left to top-right, by means of a cross-scanning module. This allows any pixel to contain contextual information from all four directions and can enhance the size of the sensory field in the  $H \times W$  plane. Sequences in each of the four directions are computed in the Spatial-wise Selective Scanning to obtain  $B, C \in \mathbb{R}^{bs \times N \times L_H \times W}$ , and  $\Delta \in \mathbb{R}^{bs \times d \times L_H \times W}$ , which in turn computes the feature map. Finally, the four sequences are merged to obtain a new sequence with the same size as the input sequence.

**Channel-wise Selective Scanning.** Although spatial features such as local texture and global structure intrinsic to 2D image features are already available through Liu et al [31]. However, in deep features, channels contain richer and diverse contextual information, which is mostly ignored by these methods. Therefore, we design a spatial and channel-based parallel scanning approach to compensate for the missing channel information in planar scanning, as shown in Fig. 3. We perform

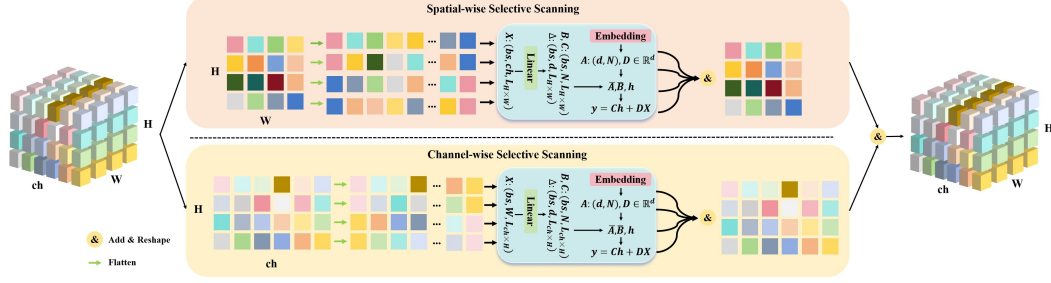


Figure 3: S3C module. In the S3C module, image features are fed into Spatial-wise Selective Scanning and Channel-wise Selective Scanning respectively. The correlation of spatial and channel dimensions in the hidden space is computed by selective state space modeling respectively. Eventually, they are merged to activate hand region features to obtain a feature map.

scan expansion and scan fusion on the  $ch \times H$  plane. First, the input features are expanded on the  $ch \times H$  plane and scanned from four directions to obtain the sequence  $X_1, X_2, X_3, X_4$ . Then, in Channel-wise Selective Scanning,  $B, C \in \mathbb{R}^{bs \times N \times L_{ch \times H}}$ , and  $\Delta \in \mathbb{R}^{bs \times d \times L_{ch \times H}}$  is calculated by Eq. 1-3 as an indication of the correlation between the feature channels. Finally, the sequences are merged and reconstructed into feature maps with the same size for images.

Image features are spatially selected by activating the mapping of each pixel in the spatial plane and the four directions of up, down, left and right to obtain local texture and structure information. In channel selection, the mapping relationship between different channels can be obtained to enhance the representation of similar channels in the implicit space in order to construct a wide range of global feature mappings and to enhance the scope of the sensory field. We visualized the range of effective receptive fields for different attentions, as shown in Fig. 1. As can be seen in Fig. 1 (d), the novel state space spatial channel attention module is able to maintain a larger and deeper receptive field and global feature mapping capability with a reduced number of parameters and linear complexity. This is consistent with our motivation to expect that enhancing the effective receptive field can better capture hand-object information associations from image features.

### 3.4 Regressor

In Regressor, we input the hand attention features obtained from S3C into it. First, a 2D heat map of each joint  $H$  is output through a simple Conv cascade. Then, a cascade of hand attention features and 2D heatmap  $HM$  is input into four residual blocks [19]. Finally, the outputs of the residual blocks are vectorized into 2048-dimensional vectors and passed to the fully-connected layer for predicting the pose parameter  $\theta \in \mathbb{R}^{48}$  and shape parameter  $\beta \in \mathbb{R}^{10}$  of the MANO. At the same time, the joint regression matrices are multiplied by the original 3D mesh  $\bar{T}$ , and the forward kinematics are applied to obtain the final 3D hand joint coordinates  $J \in \mathbb{R}^{21 \times 3}$  and the 3D hand mesh  $V \in \mathbb{R}^{778 \times 3}$ .

To train our proposed HandS3C hand mesh reconstruction model, we constrain the model by calculating L2 loss on MANO parameters, 2D hand keypoints, 3D hand keypoints and vertex coordinates.

$$\text{Loss} = \alpha_\theta \|\theta' - \theta\| + \alpha_\beta \|\beta' - \beta\| + \alpha_{2d} \|J'_{2d} - J_{2d}\| + \alpha_{3d} \|J'_{3d} - J_{3d}\| + \alpha_V \|V' - V\| \quad (4)$$

Where  $*$ ' denotes the true value,  $*$  denotes the predicted value, and  $\alpha_\theta = 10, \alpha_\beta = 0.1, \alpha_{2d} = 1e2, \alpha_{3d} = 1e4, \alpha_V = 1e4$ . the optimal solution is obtained by minimizing this objective function for training.

## 4 Experiments

### 4.1 Implementation Details

All implementations were performed with PyTorch. We used the Adam optimizer [24], and each model was trained by annealing every 10th time starting from an initial learning rate of 10-4 to train the model with batch size of 32. Both our training and testing were performed on a server with an GPU RTX A5000 (24GB). All other details will be provided in our code.

Table 1: COMPARISON WITH STATE-OF-THE-ART METHODS ON FREIHAND.

Method	Params↓	PA-MPJPE↓	PA-MPVPE↓	F@5↑	F@15↑
Hasson et al. [17]	33.5M	13.3	13.3	0.429	0.907
ExPose [7]	–	11.8	12.2	0.484	0.918
Kulon et al. [25]	519.0M	8.4	8.6	0.614	0.966
I2L-MeshNet [35]	136.8M	7.4	7.6	0.681	0.973
Pose2Mesh [6]	75.0M	7.4	7.6	0.683	0.973
Tang et al. [45]	156.5M	6.7	<b>6.7</b>	<b>0.724</b>	0.981
Junhyeong et al. [5]	153.0M	<b>6.5</b>	–	–	0.982
HandS3C (Ours)	<b>31.8M</b>	7.6	7.0	0.690	<b>0.982</b>

Table 2: COMPARISON WITH STATE-OF-THE-ART METHODS ON DEXYCB.

Method	Params↓	MPJPE↓	PA-MPJPE↓
Spurr et al. [44]	–	17.34	6.83
METRO [28]	229.5M	15.24	6.99
Liu et al. [30]	34.9M	15.28	6.58
HandOccNet [37]	39.3M	14.04	5.80
H2ONet [50]	–	14.00	5.70
Feng et al. [10]	–	13.20	5.60
HandGCAT [48]	75.8M	13.76	5.60
HandS3C (Ours)	<b>31.8M</b>	<b>12.81</b>	<b>5.52</b>

## 4.2 Datasets and Evaluation Metrics

**FREIHAND.** This dataset [54] presents the first massively diverse hand dataset containing 32,560 training samples with the possibility of replacing four backgrounds. Also, there are 3960 test samples under occlusion and poor lighting.

**DEXYCB.** This dataset [2] is a large-scale dataset for object grasping and contains 582K image frames grasped on 20 YCB objects. We use the official “S0” segmentation to evaluate the right hand pose.

**HO3D.** This dataset [15] is a hand-object interaction dataset with severe occlusion and contains 66,034 training samples and 11,524 test samples. The dataset provides RGB images with MANO-based hand joints and meshes and camera parameters. The test set provides only the annotations of the RGB images and the hand bounding box, and the test results can be evaluated through an online submission system.

Table 3: COMPARISON WITH STATE-OF-THE-ART METHODS ON HO3D.

Method	Params↓	PA-MPJPE↓	PA-MPJPE AUC↑	PA-MPVPE↓	PA-MPVPE AUC↑	F@5↑	F@15↑
I2L-MeshNet [35]	136.8M	11.2	0.775	13.9	0.722	0.409	0.932
Hasson et al. [18]	<b>13.2M</b>	11.0	0.780	11.2	0.777	0.464	0.939
Hampali et al. [15]	–	10.7	0.788	10.6	0.790	0.506	0.942
METRO [28]	229.5M	10.4	0.792	11.1	0.779	0.484	0.946
Liu et al. [30]	34.9M	9.9	0.803	9.5	0.810	<b>0.528</b>	<b>0.956</b>
I2UV-HandNet [4]	–	9.9	0.804	10.1	0.799	0.500	0.943
ArtiBoost [26]	25.3M	11.4	0.773	10.9	0.782	0.488	0.944
Keypoint [16]	56.5M	10.8	0.786	–	–	–	–
HandS3C (Ours)	31.8M	<b>9.5</b>	<b>0.808</b>	<b>9.5</b>	<b>0.810</b>	0.518	0.955

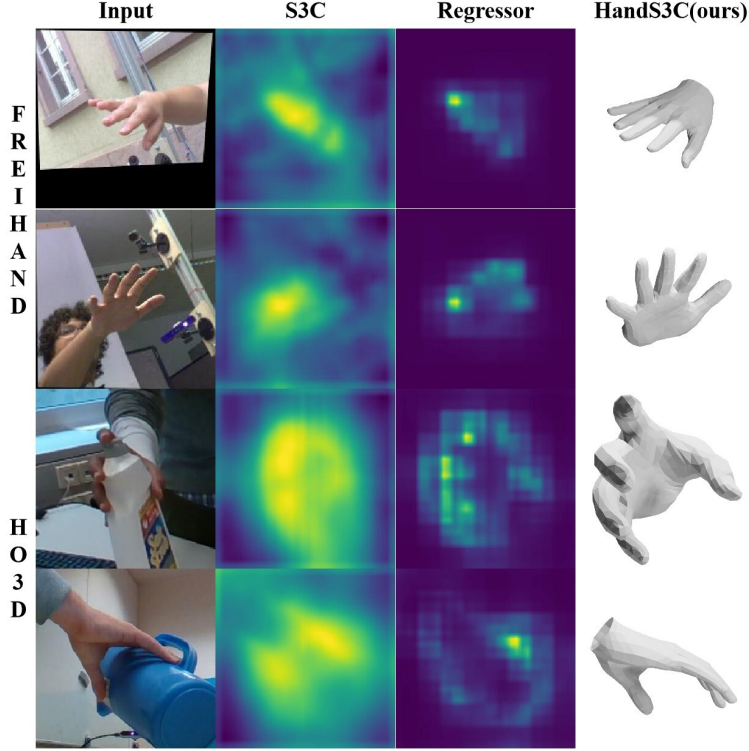


Figure 4: Qualitative results for FREIHAND and HO3D. From left to right are the input image containing severe occlusions and angular distortions, the attention mapping map obtained by S3C, the heat map of keypoints in Regressor, and the hand mesh.

Table 4: ABLATION RESULTS FOR THE FREIHAND.

Method	PA-MPJPE↓	PA-MPVPE↓	F@5↑	F@15↑
Baseline	8.0	7.4	0.669	0.977
Baseline+Self-Attention	7.7	7.0	0.688	0.981
Baseline+S3C	<b>7.6</b>	<b>7.0</b>	<b>0.690</b>	<b>0.982</b>

**Evaluation metrics.** For FreiHand, we report PA-MPJPE and PA-MPVPE in *mm* as well as F-scores. For HO3D, we report PA-MPJPE/MPVPE, AUC and F-scores returned from the official evaluation server. For DexYCB, we report MPJPE and PA-MPJPE in *mm*.

### 4.3 Comparisons with the State-of-the-art Methods

We compare our proposed method with several recent state-of-the-art methods on three datasets as shown in Tables 1-3. As can be seen from Table 1, our method maintains state-of-the-art performance in the F@15 metric on a smaller number of datasets, although it is slightly worse than the other methods in the PA-MPJPE metric [5, 45]. Moreover, its number of parameters shrinks by a factor of nearly 5 compared to models with higher accuracy [5]. On the HO3D dataset, our method reduces the

Table 5: ABLATION RESULTS FOR THE DEXYCB.

Method	MPJPE↓	PA-MPJPE↓
Baseline	14.07	5.78
Baseline+Self-Attention	14.40	5.81
Baseline+S3C	<b>12.81</b>	<b>5.52</b>



Table 6: ABLATION RESULTS FOR THE HO3D.

Method	PA-MPJPE↓	PA-MPVPE↓	F@5↑	F@15↑
Baseline	9.8	9.7	0.516	0.954
Baseline+Self-Attention (4.6M)	10.1	10.1	0.502	0.947
Baseline+SSA (0.57M)	9.8	9.8	<b>0.521</b>	0.952
Baseline+serial-S3C (0.58M)	9.9	9.8	0.516	0.952
Baseline+S3C (0.58M)	<b>9.5</b>	<b>9.5</b>	0.518	<b>0.955</b>

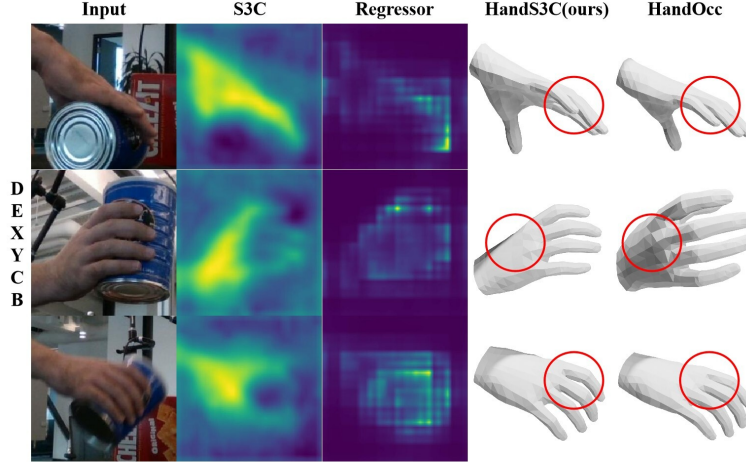


Figure 5: Qualitative results for DEXYCB. From left to right are the input image containing severe occlusions and angular distortions, the attention mapping map obtained by S3C, the heat map of keypoints in Regressor, the hand mesh and HandOCC [37] hand mesh results.

number of parameters by about 40% compared to recent methods [16]. Meanwhile, when the number of parameters is similar to the method of Liu et al. [30], all other metrics are greatly improved, and only the F-score metric is slightly reduced. To verify the effectiveness of our proposed method in the case of large-scale occlusion, the metrics on the DEXYCB dataset are shown in Table 2, and all the metrics outperform the recent state-of-the-art models [48, 50, 10]. In conclusion, the experimental results on all three datasets show that our proposed method can still be effective in estimating hand postures when a large number of occlusions are included. Moreover, the state-of-the-art performance can be maintained while reducing the number of parameters, as shown in Fig.4 - 5.

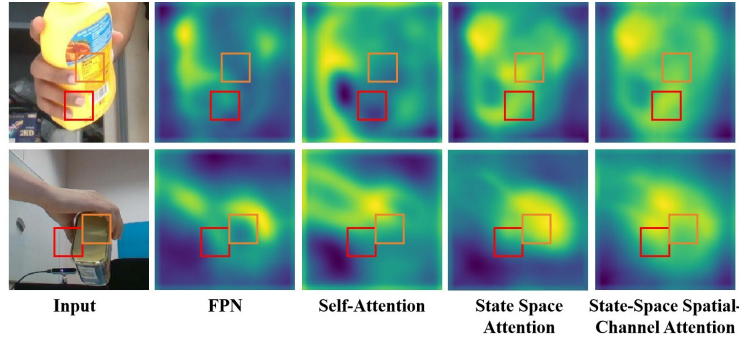


Figure 6: Attention characterization map. It is worth noting that the S3C module is able to obtain sufficient hand information in the hand interaction edge region and the occlusion region. And the method expands the range of the receptive field so that it can capture the global feature mapping. (Orange is the occluded region and red is the hand interaction edge region)



#### 4.4 Ablation Study

In order to validate the effectiveness of the HandS3C method, we further analyze the different attention modules. The results of the ablation experiments on different datasets are shown in Tables 4-6. On the FreiHand and DEXYCB datasets, we perform three experiments, i.e., Baseline, Adding Self-Attention Module, and Adding S3C Module, as a way to validate that our proposed S3C is able to expand the effective receptive field while enhancing the hand features. On the HO3D dataset, we conducted five experiments: baseline, adding a self-attention module, adding a traditional state-space attention module (SSA), adding a serial state-space spatial-channel attention module (serial-S3C), and adding a parallel state-space spatial-channel attention module (S3C). With this approach, we demonstrate that a state-space model with added channel information enhances the ability to extract hand features under occlusion, with a wider effective receptive field, and the effectiveness of the parallel structure.

From Tables 4 and 5, we can see that in the presence of occlusion on the hand, the global feature information obtained from the self-attention mechanism, although it can enhance the hand features to a certain extent, will introduce more noise information. In Fig. 6, we visualize the attention distribution map, and it can be clearly seen that the feature map tends to characterize the global information after adding the attention mechanism, but still does not extract the hand features well for the occluded regions and hand interaction edges. The SSA module, on the other hand, aggregates more hand information and performs better at the interaction edges, but it will characterize the occluded part as the hand, which introduces interference information to a certain extent. The S3C module expands the range of the receptive field through the spatial plane selection mechanism, and then directionally strengthens the hand region features through the selection of the channel planes. Furthermore, by benefiting from linear directional scanning, the occluded areas are characterized using adjacent hand information, which reduces the introduction of interference through this global mapping capability.

In Table 6, it can be found that after the introduction of the state selection of the channel plane, the number of parameters of the model is only slightly increased by 0.01M, however, a significant improvement of nearly 2% is realized in the two performance metrics of PA-MPJPE and PA-MPVPE. This is due to the fact that the state selection in the channel plane enhances the selection and fusion of image features, and is able to extract more important channel information. The current state-space model focuses more on multi-directional scanning in the spatial plane, which is the reason for the 0.3% improvement in the F@5 metrics when using SSA. Using only the spatial plane for state selection, each pixel will focus more on neighboring pixels. However, observing other metrics will show that the channel dimension in the image will then contain richer feature information, which happens to be ignored by SSA.

For the choice of serial and parallel structures, success was achieved in image restoration through serial structures in the study of Deng et al. [8]. However, since SSM resembles the linear computation of recurrent neural networks (RNN). Serial scanning in space and channel add extra computation time. Meanwhile, compared to the parallel structure, the serial structure does not balance the contributions of spatial and channel dimensions well, as shown in the ablation experiments in Table 6.

## 5 Conclusion

In order to effectively mitigate the challenges of the hand mesh reconstruction task under occlusion conditions, we introduced the state space model into the task of hand mesh reconstruction for the first time and propose the HandS3C method. The method expanded the effective receptive field and acquired hand features under occlusion by parallel cross-scanning in the spatial and channel planes. Among them, the spatial plane is able to acquire feature associations in different directions for each pixel, and the channel plane activates the target region features through state selection. This novel attention architecture is able to acquire sufficient global information and expand the effective sensory field while keeping the number of parameters small. Extensive experimental results show that this method is able to accurately predict hand postures from heavily occluded situations. Meanwhile, we expect this spatial and channel-wise state-space attention architecture to make progress in different downstream tasks.

## References

- [1] Adnane Boukhayma, Rodrigo de Bem, and Philip H. S. Torr. “3D Hand Shape and Pose From Images in the Wild”. In: *2019 IEEE/CVF Conference on Computer Vision and Pattern Recognition (CVPR)* (2019), pp. 10835–10844. URL: <https://api.semanticscholar.org/CorpusID:60440461>.
- [2] Yu-Wei Chao et al. *DexYCB: A Benchmark for Capturing Hand Grasping of Objects*. 2021. arXiv: 2104.04631 [cs.CV].
- [3] Jiayi Chen et al. *Tracking and Reconstructing Hand Object Interactions from Point Cloud Sequences in the Wild*. 2022. arXiv: 2209.12009 [cs.CV].
- [4] Ping Chen et al. *I2UV-HandNet: Image-to-UV Prediction Network for Accurate and High-fidelity 3D Hand Mesh Modeling*. 2021. arXiv: 2102.03725 [cs.CV].
- [5] Junhyeong Cho, Kim Youwang, and Tae-Hyun Oh. *Cross-Attention of Disentangled Modalities for 3D Human Mesh Recovery with Transformers*. 2022. arXiv: 2207.13820 [cs.CV].
- [6] Hongsuk Choi, Gyeongsik Moon, and Kyoung Mu Lee. *Pose2Mesh: Graph Convolutional Network for 3D Human Pose and Mesh Recovery from a 2D Human Pose*. 2021. arXiv: 2008.09047 [cs.CV].
- [7] Vasileios Choutas et al. “Monocular Expressive Body Regression through Body-Driven Attention”. In: *ArXiv abs/2008.09062* (2020). URL: <https://api.semanticscholar.org/CorpusID:221187045>.
- [8] Rui Deng and Tianpei Gu. “CU-Mamba: Selective State Space Models with Channel Learning for Image Restoration”. In: 2024. URL: <https://api.semanticscholar.org/CorpusID:269214068>.
- [9] Alexey Dosovitskiy et al. *An Image is Worth 16x16 Words: Transformers for Image Recognition at Scale*. 2021. arXiv: 2010.11929 [cs.CV].
- [10] Shuang Feng, Wenbo He, and Shaodong Li. “3D Hand Reconstruction via Aggregating Intra and Inter Graphs Guided by Prior Knowledge for Hand-Object Interaction Scenario”. In: *ArXiv abs/2403.01733* (2024). URL: <https://api.semanticscholar.org/CorpusID:268248287>.
- [11] Yao Feng et al. *Collaborative Regression of Expressive Bodies using Moderation*. 2021. arXiv: 2105.05301 [cs.CV].
- [12] Albert Gu and Tri Dao. *Mamba: Linear-Time Sequence Modeling with Selective State Spaces*. 2023. arXiv: 2312.00752 [cs.LG].
- [13] Albert Gu, Karan Goel, and Christopher Ré. *Efficiently Modeling Long Sequences with Structured State Spaces*. 2022. arXiv: 2111.00396 [cs.LG].
- [14] Albert Gu et al. *Combining Recurrent, Convolutional, and Continuous-time Models with Linear State-Space Layers*. 2021. arXiv: 2110.13985 [cs.LG].
- [15] Shreyas Hampali et al. *HONotate: A method for 3D Annotation of Hand and Object Poses*. 2020. arXiv: 1907.01481 [cs.CV].
- [16] Shreyas Hampali et al. “Keypoint Transformer: Solving Joint Identification in Challenging Hands and Object Interactions for Accurate 3D Pose Estimation”. In: *2022 IEEE/CVF Conference on Computer Vision and Pattern Recognition (CVPR)* (2021), pp. 11080–11090. URL: <https://api.semanticscholar.org/CorpusID:248240195>.
- [17] Yana Hasson et al. “Learning Joint Reconstruction of Hands and Manipulated Objects”. In: *2019 IEEE/CVF Conference on Computer Vision and Pattern Recognition (CVPR)* (2019), pp. 11799–11808. URL: <https://api.semanticscholar.org/CorpusID:106404030>.
- [18] Yana Hasson et al. *Leveraging Photometric Consistency over Time for Sparsely Supervised Hand-Object Reconstruction*. 2020. arXiv: 2004.13449 [cs.CV].
- [19] Kaiming He et al. *Deep Residual Learning for Image Recognition*. 2015. arXiv: 1512.03385 [cs.CV].
- [20] Jie Hu et al. *Squeeze-and-Excitation Networks*. 2019. arXiv: 1709.01507 [cs.CV].
- [21] Umar Iqbal et al. *Hand Pose Estimation via Latent 2.5D Heatmap Regression*. 2018. arXiv: 1804.09534 [cs.CV].
- [22] Changlong Jiang et al. *A2J-Transformer: Anchor-to-Joint Transformer Network for 3D Interacting Hand Pose Estimation from a Single RGB Image*. 2023. arXiv: 2304.03635 [cs.CV].

- [23] Zixun Jiao et al. “MTHI-former: Multilevel attention for two-handed reconstruction from RGB image”. In: *Electronics Letters* 59.23 (2023), e13040. DOI: <https://doi.org/10.1049/el12.13040>. eprint: <https://ietresearch.onlinelibrary.wiley.com/doi/pdf/10.1049/el12.13040>. URL: <https://ietresearch.onlinelibrary.wiley.com/doi/abs/10.1049/el12.13040>.
- [24] Diederik P. Kingma and Jimmy Ba. *Adam: A Method for Stochastic Optimization*. 2017. arXiv: 1412.6980 [cs.LG].
- [25] Dominik Kulon et al. *Weakly-Supervised Mesh-Convolutional Hand Reconstruction in the Wild*. 2020. arXiv: 2004.01946 [cs.CV].
- [26] Kailin Li et al. *ArtiBoost: Boosting Articulated 3D Hand-Object Pose Estimation via Online Exploration and Synthesis*. 2022. arXiv: 2109.05488 [cs.CV].
- [27] Mengcheng Li et al. *Interacting Attention Graph for Single Image Two-Hand Reconstruction*. 2022. arXiv: 2203.09364 [cs.CV].
- [28] Kevin Lin, Lijuan Wang, and Zicheng Liu. *End-to-End Human Pose and Mesh Reconstruction with Transformers*. 2021. arXiv: 2012.09760 [cs.CV].
- [29] Tsung-Yi Lin et al. *Feature Pyramid Networks for Object Detection*. 2017. arXiv: 1612.03144 [cs.CV].
- [30] Shaowei Liu et al. *Semi-Supervised 3D Hand-Object Poses Estimation with Interactions in Time*. 2021. arXiv: 2106.05266 [cs.CV].
- [31] Yue Liu et al. *VMamba: Visual State Space Model*. 2024. arXiv: 2401.10166 [cs.CV].
- [32] Wenjie Luo et al. *Understanding the Effective Receptive Field in Deep Convolutional Neural Networks*. 2017. arXiv: 1701.04128 [cs.CV].
- [33] Jun Lv et al. *HandTailor: Towards High-Precision Monocular 3D Hand Recovery*. 2021. arXiv: 2102.09244 [cs.CV].
- [34] Jun Ma, Feifei Li, and Bo Wang. *U-Mamba: Enhancing Long-range Dependency for Biomedical Image Segmentation*. 2024. arXiv: 2401.04722 [eess.IV].
- [35] Gyeongsik Moon and Kyoung Mu Lee. *I2L-MeshNet: Image-to-Lixel Prediction Network for Accurate 3D Human Pose and Mesh Estimation from a Single RGB Image*. 2020. arXiv: 2008.03713 [cs.CV].
- [36] Eric Nguyen et al. *S4ND: Modeling Images and Videos as Multidimensional Signals Using State Spaces*. 2022. arXiv: 2210.06583 [cs.CV].
- [37] JoonKyu Park et al. *HandOccNet: Occlusion-Robust 3D Hand Mesh Estimation Network*. 2022. arXiv: 2203.14564 [cs.CV].
- [38] Georgios Pavlakos et al. *Reconstructing Hands in 3D with Transformers*. 2023. arXiv: 2312.05251 [cs.CV].
- [39] Haozhe Qi et al. *HOISDF: Constraining 3D Hand-Object Pose Estimation with Global Signed Distance Fields*. 2024. arXiv: 2402.17062 [cs.CV].
- [40] Mohammad Rezaei, Razieh Rastgoo, and Vassilis Athitsos. *TriHorn-Net: A Model for Accurate Depth-Based 3D Hand Pose Estimation*. 2022. arXiv: 2206.07117 [cs.CV].
- [41] Mohammad Rezaei et al. *Pushing the Envelope for Depth-Based Semi-Supervised 3D Hand Pose Estimation with Consistency Training*. 2023. arXiv: 2303.15147 [cs.CV].
- [42] Javier Romero, Dimitrios Tzionas, and Michael J. Black. “Embodied Hands: Modeling and Capturing Hands and Bodies Together”. In: *ACM Transactions on Graphics, (Proc. SIGGRAPH Asia)*. 245:1–245:17 36.6 (Nov. 2017).
- [43] Jiacheng Ruan and Suncheng Xiang. *VM-UNet: Vision Mamba UNet for Medical Image Segmentation*. 2024. arXiv: 2402.02491 [eess.IV].
- [44] Adrian Spurr et al. *Weakly Supervised 3D Hand Pose Estimation via Biomechanical Constraints*. 2020. arXiv: 2003.09282 [cs.CV].
- [45] Xiao Tang, Tianyu Wang, and Chi-Wing Fu. “Towards Accurate Alignment in Real-time 3D Hand-Mesh Reconstruction”. In: *2021 IEEE/CVF International Conference on Computer Vision (ICCV)*. 2021, pp. 11678–11687. DOI: 10.1109/ICCV48922.2021.01149.
- [46] Ashish Vaswani et al. *Attention Is All You Need*. 2023. arXiv: 1706.03762 [cs.CL].
- [47] Rong Wang, Wei Mao, and Hongdong Li. *Interacting Hand-Object Pose Estimation via Dense Mutual Attention*. 2022. arXiv: 2211.08805 [cs.CV].

- [48] Shuaibing Wang et al. “HandGCAT: Occlusion-Robust 3D Hand Mesh Reconstruction from Monocular Images”. In: *2023 IEEE International Conference on Multimedia and Expo (ICME)*. IEEE, July 2023. DOI: 10.1109/icme55011.2023.00425. URL: <http://dx.doi.org/10.1109/ICME55011.2023.00425>.
- [49] Xiaokun Wu et al. “HandMap: Robust Hand Pose Estimation via Intermediate Dense Guidance Map Supervision”. In: *Computer Vision – ECCV 2018*. Ed. by Vittorio Ferrari et al. Cham: Springer International Publishing, 2018, pp. 246–262. ISBN: 978-3-030-01270-0.
- [50] Hao Xu et al. “H2ONet: Hand-Occlusion-and-Orientation-Aware Network for Real-Time 3D Hand Mesh Reconstruction”. In: *2023 IEEE/CVF Conference on Computer Vision and Pattern Recognition (CVPR)*. 2023, pp. 17048–17058. DOI: 10.1109/CVPR52729.2023.01635.
- [51] Xiong Zhang et al. *Hand Image Understanding via Deep Multi-Task Learning*. 2021. arXiv: 2107.11646 [cs.CV].
- [52] Zimeng Zhao et al. *Semi-supervised Hand Appearance Recovery via Structure Disentanglement and Dual Adversarial Discrimination*. 2023. arXiv: 2303.06380 [cs.CV].
- [53] Christian Zimmermann and Thomas Brox. *Learning to Estimate 3D Hand Pose from Single RGB Images*. 2017. arXiv: 1705.01389 [cs.CV].
- [54] Christian Zimmermann et al. *FreiHAND: A Dataset for Markerless Capture of Hand Pose and Shape from Single RGB Images*. 2019. arXiv: 1909.04349 [cs.CV].